SUBSONIC AND SUPERSONIC GROUND EXPERIMENTS FOR THE CALLISTO VTVL LAUNCHER DEMONSTRATOR

J. Riehmer[1], *A. Marwege*[1], *J. Klevanski*[1], *A. Gülhan*[1]
E. Dumont[2]

[1] DLR Institute of Aerodynamics and Flow Technology, Cologne, Germany
[2] DLR Institute of Space Systems, Bremen, Germany

ABSTRACT

CALLISTO is a technology demonstrator developed in a joint project of the DLR, CNES and JAXA in order to investigate VTVL technologies. This paper will give an update on ongoing wind tunnel tests in the Trisonic Wind Tunnel (TMK) at the DLR Department of Supersonic and Hypersonic Flow Technologies in Cologne for the current flight configuration. Focus is the evaluation of flow visualization techniques like schlieren imaging and oil film visualization and comparison of the experimental data with the AEDB. Flow conditions were chosen for representative flight Mach numbers of the subsonic up to supersonic flight regime; different angles of attack and the ascent as well as descent configuration were investigated. Furthermore the already presented experimental results [3] will be updated and extended by the roll moment measurements. Finally an outlook on planed experimental investigations will be given.

Index Terms— CALLISTO, VTVL, wind tunnel testing, flow visualization, aerodynamic data base

1. INTRODUCTION

In 2017 the German Aerospace Center (DLR), the French National Centre for Space Studies (CNES) and the Japanese Aerospace Exploration Agency (JAXA) joined their forces to develop, mature and demonstrate technologies for a reusable Vertical Take-off Vertical Landing (VTVL) launcher. Within the CALLISTO - Project [1] (Cooperative Action Leading to Launcher Innovation in Stage Toss back Operations) a demonstrator for a reusable vertical take-off, vertical landing stage is being developed and built. This project will culminate in several demonstration flights of the CALLISTO flight vehicle from the Kourou Space Center in French Guyana in the first half of the next decade.

The DLR is in charge of the aerodynamic and aerothermal design and characterization of the vehicle for the whole mission [2]. Especially the aerodynamic controlled part of the descent is critical and requires extensive investigations in order to build up trust in the AErodynamic DataBase (AEDB) and evaluate the uncertainties to be considered for GNC analysis. To achieve this, several detailed numerical and experimental analyses are ongoing.

2. TEST FACILITY

Tests have been conducted in the Trisonic Wind Tunnel (TMK) of the German Aerospace Center in Cologne [3]. The TMK is a blow down facility for Mach numbers ranging from 0.5 up to 5.7 in a rectangular test chamber of 0.6x0.6 m². High pressure air is blown thru an adaptable nozzle into the test chamber and released into free atmosphere via an adaptable diffusor. In order to reduce back pressure in the wind tunnel an ejector is used for low Reynolds number conditions. A schematic sketch of the wind tunnel is shown in Figure 1.

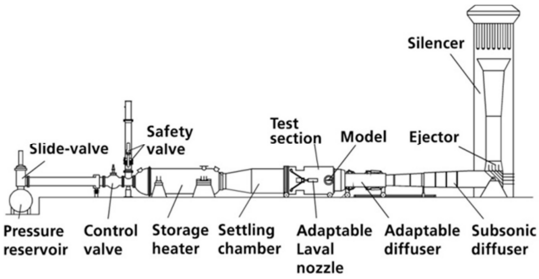

Figure 1: Schematic of TMK wind tunnel

For this test campaign subsonic and transonic (M<1.2) test were operated at static pressures of 1bar while for supersonic conditions a constant dynamic pressure of 1bar for all Mach numbers were chosen. An overview of the projected flow parameters is shown in Table 1.

Table 1: Reference wind tunnel conditions in TMK

M [-]	p_0 [bar]	T_0 [K]	q [Pa]
0.5	1.20	300	17732
0.7	1.41	300	34754
0.9	2.16	300	57451
1.3	2.37	300	85822
1.5	2.36	300	101325
2.0	2.83	300	101325
2.5	3.96	300	101325

Three subset test campaigns were conducted within this study. In the first part flow visualization with oil film techniques for subsonic transonic and supersonic flow were created. In the second test campaign the influence of Reynolds number, tripping and roll deflection was investigated for the supersonic regime. The last campaign was a continuation of the previous campaign [4?] with respect to force and moment measurements but for subsonic and transonic flow regime.

For force measurements the wind tunnel model was mounted on a rotatable sting which allowed angle of attack variations (pitching angle) of up to ±20°. During a typical run polar curves for the individual configuration and Mach number were created. Maximal angles were limited, in order to avoid contact between the sting and the balance which cause erroneous results. In order to catch a potential hysteresis effect the polar curve was created twice: first by rotating the sting (angle of attack) clockwise followed by a motion backwards in counter clockwise direction.

3. MODEL

The model characterized in the TMK is a 35:1 downscaled version of the CALLISTO. In contrast to classical rockets it has additional control surfaces on the top of the rocket and landing legs in the base region which have significant influence on the aerodynamics of the whole vehicle. It is a preliminary version labeled CAL1B with simplified outer shape in order to characterize the general flow topology.

Figure 2 shows the individual parts of the model. It has a length of approx.. 360 mm and a reference diameter of 31.43 mm. In order to investigate the ascent and descent aerodynamics, the model was construction allowed its integration in the wind tunnel in forward and backward facing direction (Figure 3).

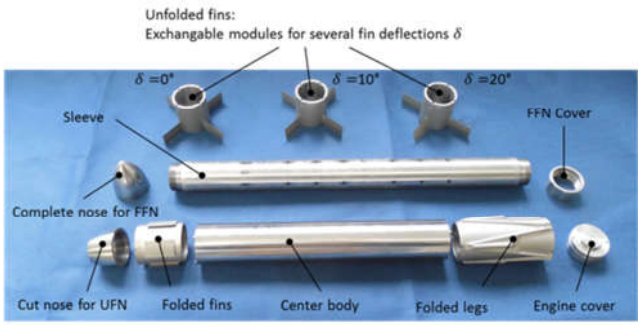

Figure 2: Disassembled CALLISTO TMK model

The forward facing orientation is named FFN and the backward facing configuration UFN. For the UFN configuration the fin module is replaced with a module with deployed fins with different angles of attack. In the present study only two modules were investigated. One module with no deflection of the fins and another one with the same deflection of all four fins of 10°, in order to generate a roll moment on the rocket.

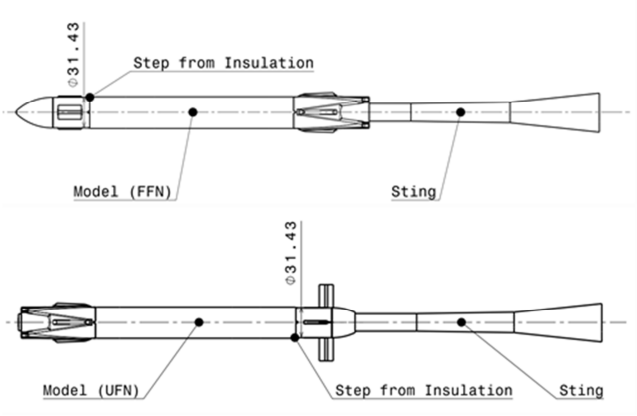

Figure 3: Sketch of TMK model on wind tunnel sting

The model was instrumented with 4 pressure ports at the interface between the model and sting, in order to measure the pressure in the wake of the base region. For force measurements a six component strain gauge floating frame balance *Task 0.75" 27330* was used. In case of oil film visualization the balance was removed in order to avoid contamination of the balance.

Optical schlieren images were used to visualize the shock patterns in the supersonic flow regime.

For a more detailed description of the wind tunnel setup and configurations further information can be found in the following papers [4,5].

Figure 4 shows the reference frame and nomenclature of the coefficients used for the aerodynamic database. The pitching moment coefficient CM which is counter clockwise around the origin and the roll moment coefficient CLF around the central axis (x-axis) of the rocket is not shown. For the pitching moment reference point a center of gravity at 60% of the vehicle was assumed and labeled as CM(COG).

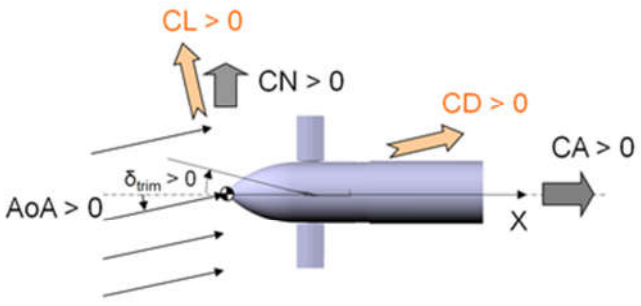

Figure 4: Reference frame used in AEDB

4. GENERAL FLOW TOPOLOGY

A short description of the general flow topology for the supersonic flow condition (M=1.5) of the UFN will be given here. Further data and detailed investigations also for the other Mach numbers can be found in more detailed in the precursor study by Marwege [4,5].

Figure 5 shows schlieren images of the first test campaign which shows shocks emerging from different parts of the rocket. Most obvious is the bow shock in front of the rocket which is detached for the UFN and attached for the FFN configuration. Going further downstream more shocks and expansion waves emerge from the landing legs of the UFN configuration and from the folded fins in the nose section of the FFN configuration. Shock reflection is visible on the top- and sidewalls but no impinging on the model occur which could influence the measurement. At the end of the rocket of the UFN configuration a strong shock is observable which originates from the side fins which are inclined to the free flow. Also flow separation and corresponding shocks in the region of the sting mounting are visible. For the FFN configuration less strong shocks emerges from the landing legs. For both configurations a flow separation like region in the leeside of rocket is visible.

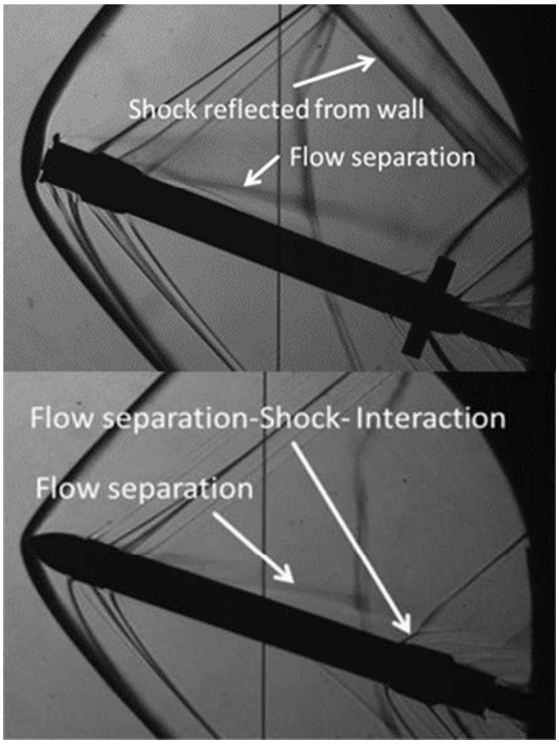

Figure 5:Schlieren imaging of UFN (AoA~160°) and FFN (AoA~20°) configuration at M=1.5

For lower Mach numbers no schlieren imaging was possible due to wind tunnel constrains but also due to absence of shocks and strong gradients which are necessary for schlieren effects.

For force measurements this study focused on the axial coefficient and the pitching moment. In Figure 6 the drag coefficient shows a nearly constant value of -1.85 for angle of attack variation between 160° and 185°. This is due to the pressure drag acting on the blunt base region of the rocket. Around 170° a slight hysteresis is observable which is even clearer in the chart below. Reason therefore could be flow separation on the fin or the central body. Further investigations are needed to determine the reason for this effect.

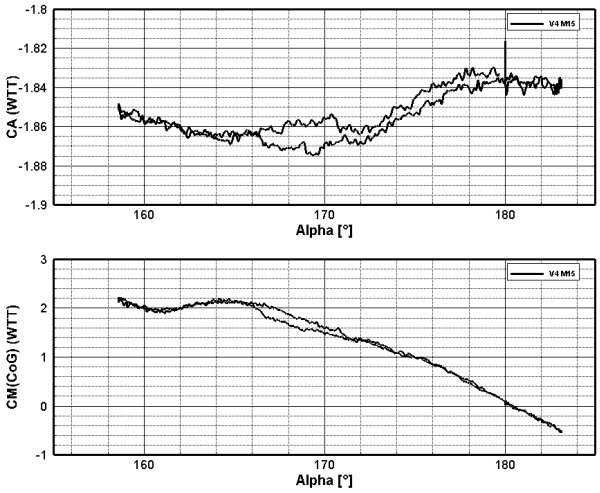

Figure 6: Drag coefficient and moment for UFN at M=1.5

The negative slope of the pitching moment curve over the angle indicates the stability of this configuration for angles of attack greater than 170. Between 160° and 165° the positive slope indicates a section where this configuration is statically unstable. Nevertheless since the center of gravity is not fixed for the CALLISTO flight vehicle this behavior may be improved throughout the project.

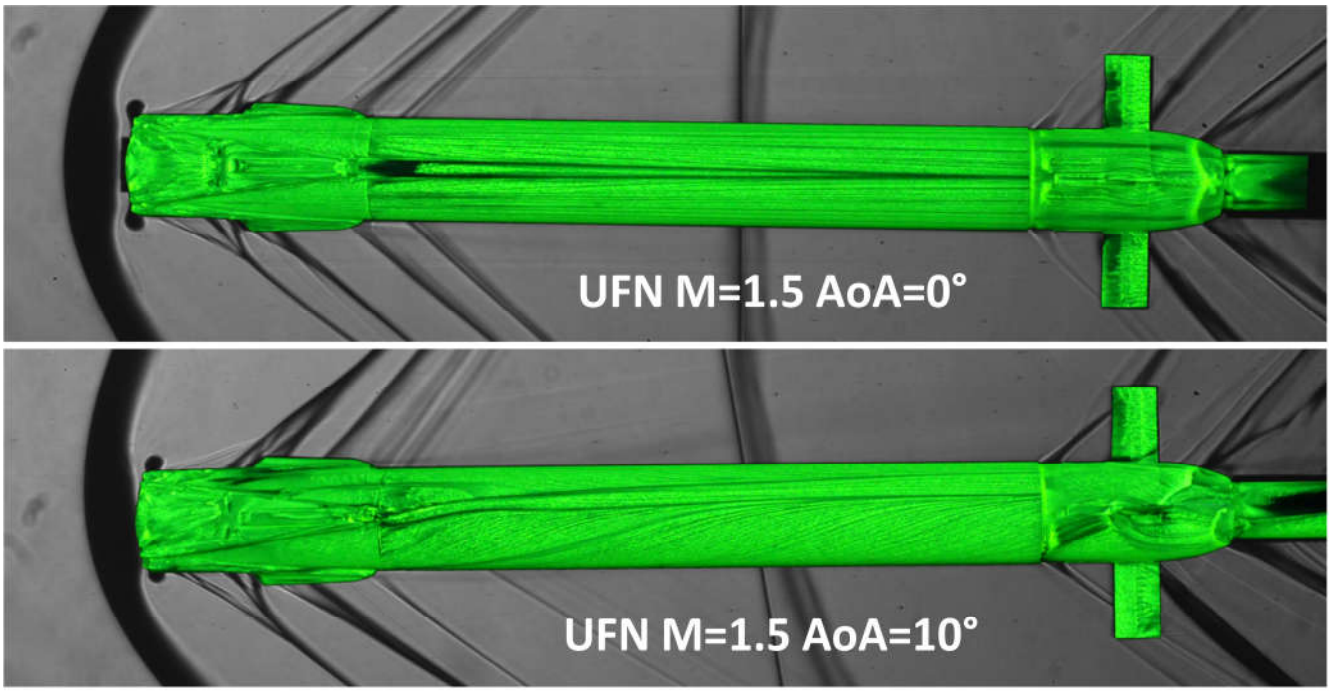

Figure 7: Combined schlieren and oil film visualization of UFN at M=1.5

5. FLOW VISUALISATION

For oil film visualization the model is painted with a mixture of oil and luminescent pigments and installed into the wind tunnel. Subsequently the model is exposed to a constant flow condition for a reasonable amount of time until oil is dried out. Afterwards the model is detached from the wind tunnel and photographed in a dedicated room under similar lightning conditions. Consequently the model was cleaned for further experimental runs.

Due to this laborious procedure only three Mach numbers (M=0.5, 0.9 and 1.5) for FFN and UFN configuration were investigated. For FFN configuration only 0° and 10° angle of attack was investigated while for UFN configuration an additional angle of 20° was investigated.

Figure 7 shows a combination of oil film and schlieren imaging at M=1.5 of the UFN configuration at AoA=0° and 10°. Clearly a detached shock in front of the base is visible and further shocks are emerging from different parts of the landing legs. A trailing wake region follows the upper part of the landing legs up to the fins. In the schlieren images a strong shock emerges from the step after the tank section and impinges on the fins but don't show visible effects on the oil film visualization. On the tip of the rocket a flow separation is clearly visible in the oil film visualization and the schlieren imaging.

For an angle of attack of 170° (resp. 10°) the landing leg shock systems varied a little but no strong changes are visible. On the fuselage the stream lines are bending upwards and the landing leg wake region also moves upwards and increases in size. Significant changes are seen in the top part of the rocket. It seems that a further separation emerged from the wing and is connected to the one emerging from the tip. This complex structure may the reason for the hysteresis effects mentioned before.

6. ROLL MOMENT

An important part of this study was to assess the roll moment of the vehicle. Therefore the fin module was replaced with a module where all 4 fins were deflected to 10°.

Figure 8 shows the coefficient at different angles of attack for the supersonic Mach numbers 1.5, 2.0 and 2.5. For the dotted lines the model was rotated by 45° in the roll axis in order to investigate the effect when all for fins are exposed to the flow at the angle of attack.

Generally the effect of roll deflection decreases with higher Mach numbers and is nearly double for M=1.5 in comparison to M=2.5. The effectiveness of the roll moment in dependency of angle of attack changes significantly but with no obvious trend. For high Mach numbers the roll moment increases with higher angle of attack while for

M=1.5 the roll moment decreases. At Mach 2.0 and angle of attack of 160° hysteresis is observable. Overall the curves show a very "bumpy" behavior which indicates very complex flow structures in the fin area which is also visible in the flow visualization pictures (Figure 7). The symbols in the same plot are values extracted from the CALLISTO AEDB for the corresponding flow conditions. For no angle of attack (180°) the values of experiment and database show very similar results. As soon as the angle of attack is increased the agreement decreases and differences between AEDB and experiments increases up to 15% for all Mach numbers. Nevertheless the trend of all curves is well predicted by the AEDB.

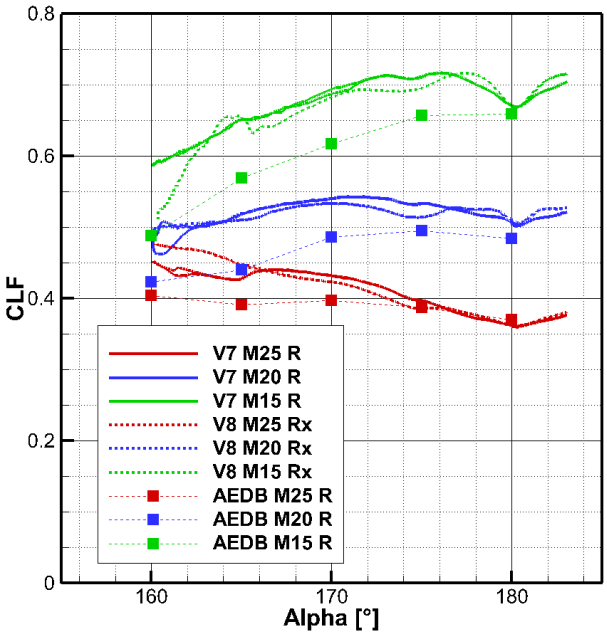

Figure 8: Roll moments for UFN configuration

In Figure 9 for Mach 1.5 the case with no deflection (V4 M15) and 10° deflection of all fins are plotted (V7 M15 R). The general shape is only influenced slightly but the drag coefficient is increased by ~10%. The pitching moment is reduced by approximately 0.2 for higher angle of attacks (AoA<178°) but also keeps the general trend of the polar without roll fin deflection.

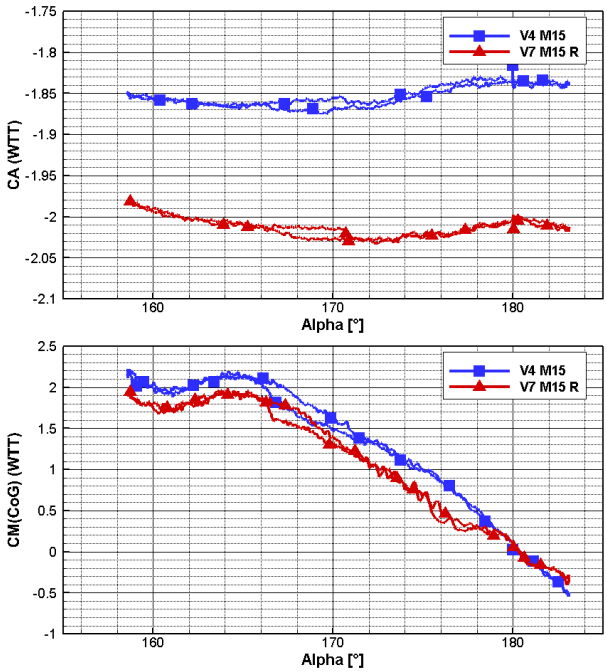

Figure 9: Influence of roll fin deflection on coefficients

7. REYNOLDS NUMBER INFLUENCE

Since the TMK wind tunnel cannot reproduce the Reynolds number of the expected real flight condition of CALLISTO a Reynolds number sensitivity analysis was performed. Therefore for supersonic Mach numbers of 1.5 and 2.0 a test was performed with the use of the ejector system which reduced the Reynolds number to the half. Table 2 shows the Reynolds number for the wind tunnel conditions and the reference conditions for the real flight. It can be seen that the Reynolds number based on diameter as characteristic length in the wind tunnel is nearly one order of magnitude lower than as the expected values for the real flight.

Table 2: Similarity numbers for Reynolds number variation

		Flight	TMK	TMK+Ej
M=1.5	**Re_1 [1/m]**	$8.3 \cdot 10^6$	$3.7 \cdot 10^7$	$1.8 \cdot 10^7$
	Re_d [-]	$9.1 \cdot 10^6$	$1.2 \cdot 10^6$	$0.6 \cdot 10^6$
M=2.0	**Re_1 [1/m]**	$8.0 \cdot 10^6$	$3.8 \cdot 10^7$	$1.9 \cdot 10^7$
	Re_d [-]	$8.8 \cdot 10^6$	$1.2 \cdot 10^6$	$0.6 \cdot 10^6$

In Figure 10 the results are plotted for both Mach numbers and show a very similar behavior of the low (marked with EJ) and high Reynolds number conditions. For Mach 2.0 a slightly lower pitching moment is observed for angles of attack around 166° but is within the uncertainties

of the measurement. The effect on drag and lift is smaller and therefore is not presented in this paper.

These results show that the Reynolds number variation in this range has a minor effect on the investigated cases. But the Reynolds number in real flight is expected to be one order of magnitude higher. This may change the impact and therefore extrapolation from wind tunnel data to flight conditions needs further investigation.

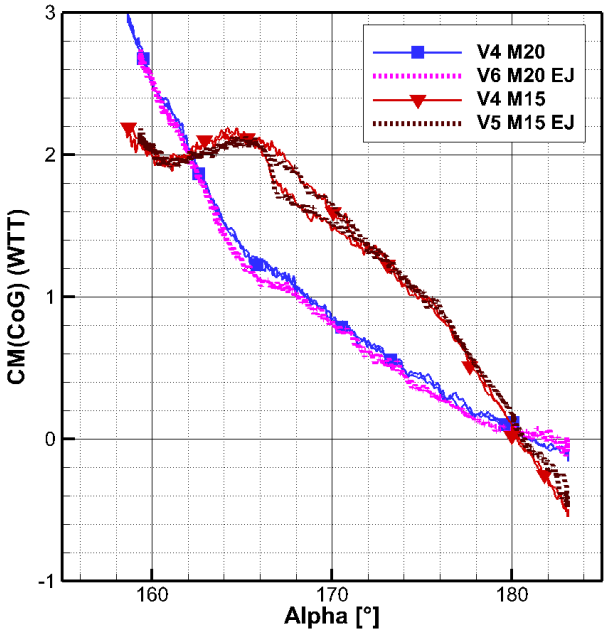

Figure 10: Reynolds number influence on pitching moment

7. BOUNDARY LAYER TRIPPING

With the boundary layer tripping it was tried to influence and to delay boundary layer separation and trigger laminar-turbulent transition. Therefore two different positions where chosen to for the application of the tripping devices. In the first runs a strip of grains on the first wedge of the fins as it is shown in Figure 11 was used. Hereby only an opposing pair of fins where modified on both sides of the individual fin. For the second tripping configuration tripping devices were applied circumferential around the fuselage right behind the landing gear as it is shown in Figure 12.

In order to apply the tripping the corresponding locations were coated with glue and silicon carbide grain were applied. A preliminary assessment of grain sizes and boundary layer thickness was performed but not further preceded since boundary layer thickness could not be assessed due to the complex flow structure and different typical grain sizes were used.

Three different size types of grain produced by ESK-SIC GmbH were used and applied to the model. The sizes where F 80 (~150µm), F 220 (~45µm) and F 320 (~37µm) (Remark: grain size and identification id are invers correlated)

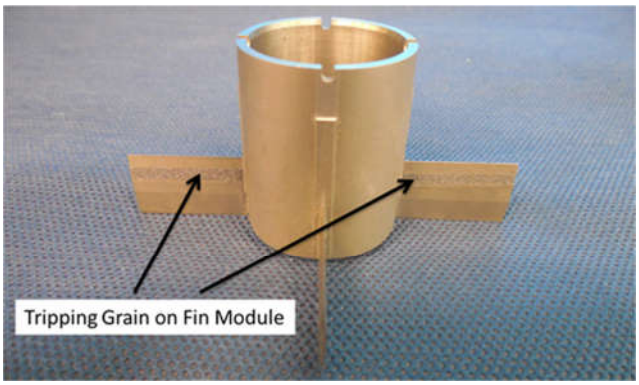

Figure 11: Tripping elements on fin module

Figure 12: Tripping elements on fuselage of CALLISTO

The influence of tripping is most obvious in the pitching moment curve therefore analysis is focused on these plots. Figure 13 shows the influence of tripping of the boundary layer on the fin for M=1.5 and M=2.0. In general only small differences can be seen and these are within the uncertainties of the measurement. For M=1.5 (thicker lines) at angles lower than 165° there seems to be a small increasing of the pitching moment for the cases with tripping elements. The strong fluctuation in the pitching moment at 176° and 178° where not repeatable and are most likely due to some fluctuations in the flow conditions.

In the M=2.0 case there seems to be a systematic influence of the tripping which increases the pitching moment with increasing grain sizes for angles between 165° and 175°. This is a behavior which would be expected for a delayed boundary layer separation expected on the leeside of the fins due to forced transition, but cannot be proved by this data alone.

For the tripping of the boundary layer circumferential to the fuselage a strong influence can be observed in Figure 14 for M=1.5 conditions. Here at lower angles (<170°) the pitching moment increases for the tripped case significantly

by a factor of 10% and also it seems that the hysteresis effect at 168° is slightly decreased with the use of the tripping devices. Different mechanisms are possible and cannot be pinned down only by the presented data. Most likely the boundary layer is tripped and get turbulent and alters the separation region along the fins and tip area of the rocket. Alternative the wake of the landing legs (see Figure 7) is modified and changes the flow field.

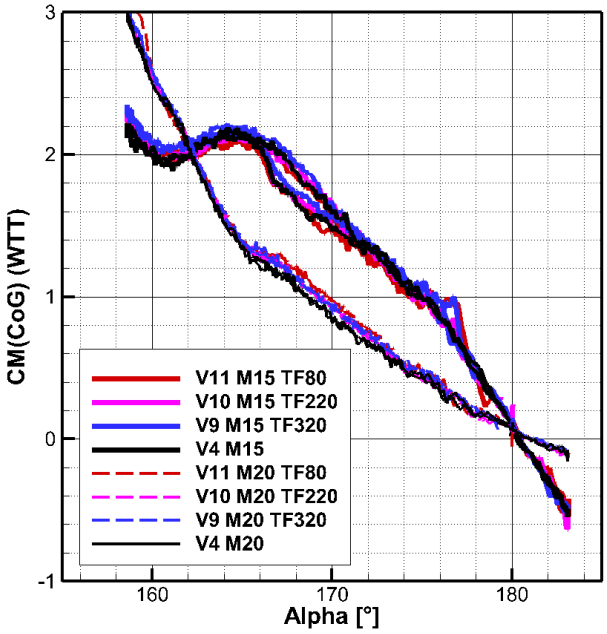

Figure 13: Influence on fin flow tripping on the overall pitching moment

A pressure drag effect of the additional grains can be ruled out since this would give a grain size dependent increase of pitching moment which is not observable from the data shown in Figure 14. This also gives confident in the grain size selection which is within the boundary layer thickness at least for the fuselage part of the vehicle.

For the M=2.0 case a small dependency seems to be visible for angle of attacks less than 160° but is within the uncertainty of the measurement.

A further analysis from the tripping investigation can be performed with respect to influence of perturbations on the overall aerodynamics. By scaling the grain sizes with the model scaling we get perturbations in the order of 5.25 mm (F 80), 1.56 mm (F 220) and 1.3 mm (F 320).

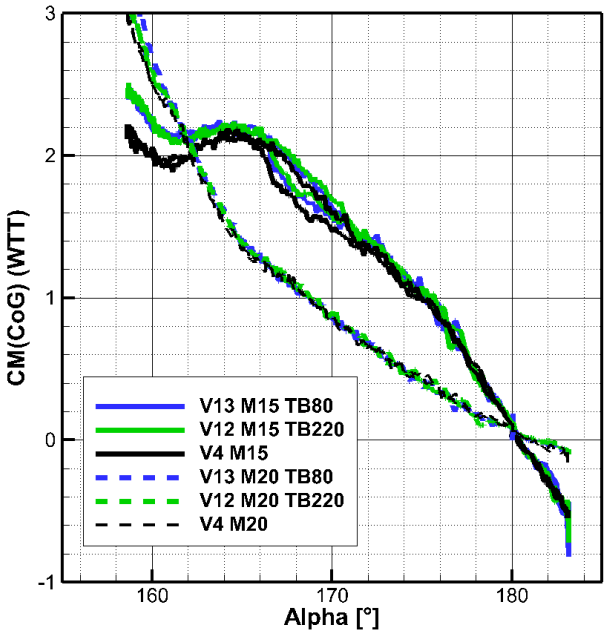

Figure 14: Influence on body flow tripping on the overall pitching moment

8. CONCLUSION & OUTLOOK

An extensive experimental study was conducted for a small scale version of the CALLISTO flight experiment in the Trisonic Wind Tunnel (TMK) at the supersonic and hypersonic technologies department at the DLR in Cologne and gave a large experimental database for further investigations and comparisons. The obtained data contained flow visualization with schlieren images for supersonic cases and oil film visualization for subsonic up to supersonic regime. From these data a good understanding of the flow structures around and along the vehicle could be derived. Force measurements on the other hand gave valuable data for comparison with the data of the AEDB created with numerical tools. Especially the roll moment coefficient showed a complex behavior and deviates from the numerical predictions. The focus of this paper was the quantification of different model and flow influences on the general forces and moments of the vehicle. Here it could be shown that there is a small influence of the results with changing Reynolds number and surface roughness elements in Reynolds variation by a factor of two. Further study necessary to predict the impact at real flight Reynolds numbers, which are on order of magnitude higher.

In future investigations the configuration will be adapted to the current CALLISTO design called CAL1C including a more detailed layout of the outer shape including protrusions like pipes, flanges, isolation, etc. Experiments in

larger facilities with Reynolds numbers closer to the real flight conditions are planned and will give a broader database for the creation and comparison with the CALLISTO AEDB.

9. ACKNOWLEDGMENTS

The authors would like to thank the technical stuff of the TMK facility Martin Achner and Daniel Habegger for their support and technical expertise during the conduction of the experiments.

12. REFERENCES

[1] E. Dumont, et al. “CALLISTO - Reusable VTVL launcher first stage demonstrator”, Space Propulsion Conference 2018, Sevilla

[2] J. Klevanski, et al “Aerodynamic Studies in Preparation for CALLISTO - Reusable VTVL Launcher First Stage Demonstrator” 69th International Astronautical Congress 2018, Bremen.

[3] H. Esch “Die 0.6-m x 0.6-m – Trisonische Meßstrecke (TMK) der DFVLR in Köln-Porz“ DFVLR-Mitt. 86-21, 1986, Cologne.

[4] A. Marwege, et al. “First Wind Tunnel Data of CALLISTO – Reusable VTVL launcher first stage demonstrator”, EUCASS 2019, Madrid

[5] A. Marwege, et al “Wind Tunnel investigations in CALLISTO - Reusable VTVL Launcher First Stage Demonstrator” 70th International Astronautical Congress 2019, Washington